AJRCMB Articles in Press. Published on 10-May-2017 as 10.1165/rcmb.2016-0242OC

Hepatic steatosis accompanies pulmonary alveolar proteinosis

Alan N Hunt[1], Anagha Malur[4], Tual Monfort[2], Pavlos Lagoudakis[3], Sumeet Mahajan[2], Anthony D Postle[1] and Mary Jane Thomassen[4]

[1]Clinical & Experimental Sciences, Faculty of Medicine, University of Southampton, Southampton SO16 6YD, UK, [2]Institute for Life Sciences & [3]School of Physics and Astronomy, University of Southampton, Southampton SO17 1BJ, [4]Division of Pulmonary, Critical Care and Sleep Medicine, Brody School of Medicine, East Carolina University, Greenville, NC 27834, USA

Conception and design: AH, AP; Experimental, data collection and observations: AH, AM, TM, PL; Data analysis and interpretation: AH, SM, AP, MT; Drafting the manuscript for important intellectual content: AH, AP, MT

Correspondence

Dr Alan N Hunt

Clinical & Experimental Sciences

Faculty of Medicine

Room LF75, Level F, South Block,

Southampton General Hospital

Tremona Road

Southampton SO16 6YD

United Kingdom

Email anh@soton.ac.uk

Tel +44 (0)2381 204178

Abstract

Maintenance of tissue-specific organ lipid compositions characterises mammalian lipid homeostasis. Lung and liver synthesise mixed phosphatidylcholine (PC) molecular species subsequently "tailored" for function. Lungs progressively enrich disaturated PC (DSPC) directed to lamellar body (LB) surfactant stores prior to secretion. Liver accumulates polyunsaturated PC directed to VLDL assembly and secretion, or triglyceride stores. In each tissue, selective PC species enrichment mechanisms lie at the heart of effective homeostasis. We tested potential coordination between these spatially separated, but possibly complementary phenomena under a major derangement of lung PC metabolism, Pulmonary Alveolar Proteinosis (PAP), which overwhelms homeostasis leading to excessive surfactant accumulation. Using static and dynamic lipidomics techniques we compared (i) tissue PC compositions and contents and (ii) in lungs, the absolute rates of synthesis from both control mice and the GM-CSF knockout model of PAP. Significant DSPC accumulation in BALF, Alveolar Macrophage (AM) and lavaged lung tissue occurred alongside increased PC synthesis consistent with reported defects in AM surfactant turnover. However, microscopy using oil red O staining, CARS, SHG and TEM also revealed neutral lipid droplet accumulations in alveolar lipofibroblasts of GM-CSF KO animals suggesting lipid homeostasis deficits extend beyond AMs. PAP plasma PC composition was significantly PUFA-enriched but content was unchanged and hepatic PUFA-enriched PC content increased by 50% with an accompanying micro/macrovesicular steatosis and a fibrotic damage pattern consistent with NAFLD. These data suggest a hepato-pulmonary axis of PC metabolism coordination with wider implications for understanding and managing lipid pathologies where compromise of one organ has unexpected consequences for another.

Keywords

Phosphatidylcholine; pulmonary surfactant; lipidomics; lipotoxicity; pulmonary alveolar proteinosis; remodelling; hepatic steatosis; CARS microscopy

AJRCMB Articles in Press. Published on 10-May-2017 as 10.1165/rcmb.2016-0242OC

Introduction

Cell functions are underpinned, in part, by tight homeostatic control of membrane phospholipid metabolism (1). Regulated at the levels of synthesis, degradation and transport, the cumulative consequences of even very small imbalances in one or more parameters are potentially catastrophic if uncorrected (1). Equilibrium maintenance requires that change in any parameter is matched by a corresponding alteration in the others. Discordance in these mechanisms will lead to either deficit or excess of membrane lipid. In the former case cell integrity and viability is compromised, in the latter the aberrant accumulation of membrane phospholipid is often accompanied by lipotoxicity.

Lipotoxicity represents a general failure of lipid homeostasis, at the excess extreme, whereby ectopic accumulation of lipid droplets occurs in lean tissue. It is most frequently reported in the contexts of overfeeding or Metabolic Syndrome (2). Excess lipid, predominantly triacylglycerol (TAG) and cholesterol esters (CE), accumulates in major organs including heart, kidney and liver as well as skeletal muscle and other tissues (3). Sequelae can include cardiomyopathy (4), renal failure (5), cirrhosis (6) and sarcopenia (7). Mechanisms underlying impairments of affected cell functions include free fatty acid-mediated ER stress, ceramide formation or oxidative damage leading to inflammation, apoptotic or necrotic cell death and fibrosis.

Most animal models of lipotoxicity involve dietary manipulation and over-feeding. For example, excessive calorie load and obesity in rodents results in excess lipid droplet accumulation within hepatocytes (6, 8). This has been used as a model of the pathology seen in human Non Alcoholic Fatty Liver Disease (NAFLD) (9). Other lipotoxicities are modelled by targeted derangement and enforced imbalance of key regulatory elements of the lipid metabolism-related genome. One established human lung lipotoxic pathology is Pulmonary Alveolar Proteinosis (PAP), characterised by an excessive accumulation of lipid rich surfactant in the alveolar compartment (10). The most common form of PAP is autoimmune in origin (11) and antibody blocking of Granular Macrophage Colony Stimulating Factor (GM-CSF) actions is the key feature of the disease process. Construction of a murine model by genetic ablation of GM-CSF recapitulated the major elements of the human PAP phenotype including the significantly deranged lung lipid homeostasis (12, 13). Much subsequent PAP research with this model has been lung-focused, concentrated on the excessive

surfactant accumulation and lipotoxic overload of alveolar macrophages (AM). The AM accretion of lipid is attributed to compromised catabolic capacity (10) and affected signalling cascade(s) downstream of GM-CSF involving PPARγ have been extensively characterised (14, 15).

PAP investigations have not explored possible lipotoxic involvement in lung cell types other than AM or indeed more systemic consequences beyond the lung. Nevertheless, other lung pathologies show lipotoxic susceptibility in different lung cells. For example in the lungs of obese (fa/fa) Zucker rats where ectopic lipid accumulates within alveolar interstitium and lipofibroblasts as well as AMs (16). Transgenic models reinforce this understanding. The targeted activation of sterol-response element-binding proteins (SREBP) in pulmonary surfactant-producing alveolar type II (AT2) cells increases alveolar surfactant but leads to a neutral lipid accumulation in AT2 cells (17). By contrast blocking of SREBP action in these cells by deleting the SREBP cleavage-activating protein gene, SCAP, in lung epithelia reduces AT2 surfactant synthesis but results in a localised neutral lipid accumulation focused on lung lipofibroblasts (18).

Possible PAP involvement in a systemic as well as local derangement of lipid homeostasis is important in the light of recent insights to AT2 cell surfactant metabolism (19). AT2 cells specialise in the synthesis, enrichment and transient accumulation/storage, prior to secretion, of saturated phosphatidylcholine (PC) as the major lipid component of pulmonary surfactant (20). We showed that the absolute amounts of lung PC normally synthesised *in vivo* exceed surfactant requirements by at least an order of magnitude (19) with the excess unsaturated PC, not destined for alveolar secretion, being returned to the circulation and presumably redirected to the liver via HDL. It is likely, therefore, that shifts in PAP whole lung surfactant PC metabolism may result in changes in circulatory PC flux with systemic consequences.

Here we have explored PAP PC metabolism using detailed static and dynamic lipidomic technologies (19). We coupled these with lipid-focused histology to probe lung and liver responses to GM-CSF knockout. We employed microscopic techniques including Oil Red O (ORO) staining and Transmission EM (TEM) along with more specific imaging techniques such as coherent anti-Stokes Raman Scattering (CARS) for lipids and second harmonic generation (SHG) for collagen fibres. Alongside established AM lipotoxicity we record significant whole lung tissue lipid accretion and

AJRCMB Articles in Press. Published on 10-May-2017 as 10.1165/rcmb.2016-0242OC

associated fibrotic damage. We identify for the first time a distinctive hepatic lipotoxic phenotype including fibrotic damage consistent with GM-CSF ablation effects extending systemically to affect aspects of whole body lipid metabolism.

Materials and methods

Studies were conducted in conformity with Public Health Service Policy on humane care and use of laboratory animals and were approved by the East Carolina University institutional animal care and use committee. The GM-CSF KO mice have been previously described (12, 13). Animals studied were age (8–12 wk old) and gender matched to wild-type C57Bl/6 controls obtained from Jackson Laboratory (Bar Harbor, ME). Eight or more mice per group were used except where indicated.

Mice were injected i.p. with 0.1mg D9-choline (Sigma-Aldrich) (19) for 3h. At sacrifice lungs were lavaged (5 x 1ml) and bronchoalveolar lavage fluid (BALF) was collected. Cells from BALF were harvested by centrifugation and frozen with a portion retained for differential cell count. Lavaged lungs, livers and plasma were snap frozen in liquid nitrogen and stored at -80°C.

Tissues for TEM were finely diced (2mm cubed) and collected into 4% formaldehyde, 3% glutaraldehyde in 0.1 M PIPES buffer. After 5 days and two buffer washes in 0.1M PIPES pH 7.2 samples were transferred to 1% OsO_4 in 0.1 M PIPES pH 7.2 for 1h, washed (x2), transferred to 2% aqueous Uranyl acetate for 20 mins and then dehydrated through successive washes in 30%, 50%, 70%, 95% and absolute ethanol. Following transfer to acetonitrile for 10 mins samples were incubated overnight in acetonitrile:resin (50:50). After a final incubation in resin for 6 hours they were embedded in fresh resin polymerised at 60°C for 24h.

For other microscopy, unfixed tissue was allowed to come to the ambient temperature of the cryostat. Tissue was mounted in OCT Embedding Matrix (CellPath). Sections, 7μm for ORO staining and 25μm for CARS/SHG were cut and were prepared onto APEs coated glass slides. ORO slides were air dried, washed and stained with ORO solution then counterstained with Mayer's Haematoxylin. Photomicrographs were collected via a Nikon microscope with 100x oil immersion objective

CARS and SHG slides were air dried, PBS was added, a coverslip placed on top and sealed with nail varnish. Images were acquired with a home-built CARS and SHG capable, multiphoton

microscope setup (21). For SHG the 835nm pump beam served as the excitation. Up to 30mW of average power from both the pump and the Stokes source was delivered to the sample with no photodamage. Samples were imaged with identical laser intensity. SHG and CARS signals, passed through suitable dichroics and narrow bandpass filters, were detected in the backward-direction using a non-descanned geometry with photomultiplier tube (PMT) detectors simultaneously in two separate channels. SHG signals were collected using a band pass filter at 420 ($\pm$10) nm. Image collection was carried out using ScanImage3.6 (Janelia Farms, Ashburn, VA). Image processing and analysis was carried out using ImageJ (22).

Lipidomic analyses including calculations of absolute rates of lung tissue PC synthesis were undertaken as described (19, 23, 24).

Unpaired t-tests were used for statistical analyses. Values were routinely expressed as the mean ± Standard Error of Mean (SEM) with p values for significance as indicated for each experiment.

Results

Lung compartment PC contents and molecular species compositions

In agreement with, previous observations (13, 14), GM-CSF ablation increased the PC recovered from BALF supernatant after cell removal. A 7.5 fold increase ($p = 0.0024$) compared with controls (Figure 1). The PC molecular species composition profiles were unsurprisingly particularly enriched in the disaturated species, predominantly PC16:0/16:0 (Figure 2A), characteristic of surfactant.

Following careful washing to remove pelleted surfactant, the PC content of cells recovered from the BALF of these affected animals, predominantly lipid-engorged macrophages, was elevated around 25 fold, $p<0.0001$ compared with controls (Figure 1). This vast excess of intracellular PC in BALF cells was also characterised by specific enrichments of DSPC and monunsaturated molecular species consistent with surfactant accumulation but also reflected a significant extracellular pool of surfactant that could not be removed by washing (Figure 2B). Other, characteristically cell membrane-related PC species, were much diminished in proportional representation.

AJRCMB Articles in Press. Published on 10-May-2017 as 10.1165/rcmb.2016-0242OC

The PC content of extensively lavaged lung tissue was also elevated 2.79 fold (Figure 1) p=0.024 indicating significant intracellular PC retention. MS analysis of lipid extracts of post-lavage lungs from GM-CSF ablated animals revealed that this residual lung PC pool was also proportionally enriched in DSPC (Figure 2C) implying a steady-state increase in surfactant PC retention/storage. This was considered most likely to be in the form of more LB storage, although some contribution in knockout animals from extracellular surfactant resistant to the extensive lavage protocol could not be excluded.

Additional data (Figure E1) showed that lavaged lung tissue PE was unaltered in GM-CSF KO animals both in content and composition. There was some significant variation in the proportions of PI molecular species with significantly more PI16:0/22:6 PI in the PAP animals. PG and PS compositions were unaltered (data not shown) but no quantitation was undertaken for these phospholipids or PI.

Lung PC synthesis and alveolar secretion

We previously established that the normal absolute rate of mouse lung PC synthesis *in vivo* far exceeds that required for surfactant secretion alone (19) and that the excess PC was likely subject to the basolateral route of removal (25). Here, using a similar D_9-choline labelling protocol, we determined the absolute PC synthesis rate in control lung over 3h *in vivo* to be 1.582 ± 0.511 μmoles PC/g wet weight lavaged lung. In GM-CSF ablated animals this was significantly higher at 4.235 ± 1.444 μmoles PC/g wet weight lavaged lung (mean ± SEM, n = 4 and 12 respectively) p = 0.0037.

The calculated deuteriated surfactant PC secretion rate into the BAL fluid of control animals at 3h, was more than an order of magnitude smaller than the synthesis rate, consistent with previous work (19), but an equivalent calculation for GM-CSF KO animals was unreliable. Deuteriated DSPC was present at low level in BALF, indicating secretion of newly synthesised surfactant 3h but, due to a much larger “dilution” of the stable isotope with the excess unlabelled BALF PC and consequent sensitivity limitations, no further meaningful inference was possible. We could not assess whether secretion rates were altered in the GM-CSF knockout animals.

Plasma

Plasma lipid composition was evaluated. However, steady state total plasma PC content showed an essential identity between both GM-CSF knockout and control animals (data not shown). The proportions of PC16:0/22:6 and PC18:0/22:6 were both significantly elevated ($p<0.02$) in GM-CSF KO animals (Figure E2). Neutral lipid analyses evaluating circulating cholesterol ester, DAG or TAG profile and content variations did not reveal any differences between groups (data not shown). The analyses of the deuteriated plasma PC profiles were uninformative following 3h of labelling with D9-choline since this is not an optimal time point for undertaking such analysis. While the possibility that greater variation in lipid profile distribution between different lipoprotein particles may exist or some variation in absolute flux through specific lipoprotein vectors including HDL may be evident, our data did not and cannot attempt to address these possibilities.

Livers

The 50% increase in liver tissue PC content of GM-CSF ablated animals from 8.31 ± 0.86 μmoles/g wet weight in controls to 12.50 ± 0.62 μmoles/g wet weight (mean ± SEM, n = 9 & 20), p = 0.001, was an unexpected finding and is a novel observation. The unsaturated nature of normal liver PC composition is well-established (24), founded on PC synthesised via N-methylation of liver phosphatidylethanolamine (26) that supports the hepatic synthesis of VLDL (26). In control animals, as anticipated, we found the liver tissue PC molecular species composition is already a mostly unsaturated lipid pool consistent with previous work (24, 26). The accumulated PC content that accompanies GM-CSF ablation resulted in a fractional super enrichment of PC16:0/18:2, PC16:0/22:6 and PC18:0/22:6 with an apparent fall in saturated and monunsaturated molecular species (Figure 3A). However, when the same species are presented in content terms (Figure 3B) it is strikingly clear that the saturated and monunsaturated species are actually statistically unchanged in abundance and that PUFA containing PC species are solely responsible for the additional PC mass present in GM-CSF livers.

Supplementary data (Figure E3) showed that elevate liver PE content and super enrichment of PUFA species was apparent consistent with a larger pool availability for PE N-methylation route of hepatic PC synthesis.

AJRCMB Articles in Press. Published on 10-May-2017 as 10.1165/rcmb.2016-0242OC

Lipid-focused tissue histology

Having identified PC accumulations in both lung and liver tissues of GM-CSF KO, we investigated the spatial distribution of lipids within both. The potential lipotoxic pathology was probed using (i) ORO staining for identifying neutral lipid droplets accumulation, (ii) CARS microscopy to provide semi-quantitative spatial characterisation of lipid droplets, (iii) SHG to identify any collagen associated with fibrotic changes and (iv) TEM for a detailed intracellular view of lipid droplet distribution.

ORO staining of neutral lipid

ORO staining of lavaged lung sections (Figure 4A & 4B), which does not routinely stain the surfactant-containing LBs due to their lack of neutral lipid content, identified sporadic neutral lipid-rich droplets in control lungs (Figure 4A). These were likely associated with lipofibroblasts (19) and there was no evidence of widespread neutral lipid accumulation in either alveolar type I (AT1) or AT2 epithelial cells. In contrast, substantial lipid droplet accumulations in epithelial cells of the GM-CSF KO animals were evident (Figure 4B) although clearly identifying whether this affected AT1, AT2 or lipofibroblast cells or both required TEM (see below).

Similar staining of liver sections showed a characteristic pattern for normal mouse liver (Figure 4C) where the vast bulk of similarly sized neutral lipid droplets were seen in the extracellular spaces, likely representing VLDL newly secreted from hepatocytes destined for the circulation. Comparable patterns of ORO staining in wild type mouse liver have been reported previously (8). Following GM-CSF ablation, however, the liver neutral lipid content was much more heavily stained with ORO (Figure 4D) with significant intracellular deposition and with a clear steatosis that shared appearance characteristics of both microvesicular steatosis and the more common macrovesicular steatosis (8).

CARS microscopy

CARS microscopy is an imaging technique increasingly utilised in biomedical applications (27). It has been widely applied for imaging lipids and their structures in cells and tissues. It provides a non-invasive, non-destructive and label-free modality to selectively image lipids in intact cells and

tissue without the use of complex procedures for sample preparation and histopathological examination. Examples of its use include in differential diagnosis of lung carcinoma (28) and for quantification of hepatic lipid in liver tissue (8). For liver has been shown that CARS can successfully evaluate hepatic microvesicular steatosis, by detection and quantification of lipid droplets, their number and size (29). Moreover CARS signal intensities from lipid droplets are consistent with their neutral lipid content and CARS microscopy is more sensitive than ORO analyses.

We examined lavaged lung tissue and corresponding liver tissue sections of control and GM-CSF KO animals with CARS. The images presented in Figures 5 & 6 show an increased amount of lipid droplets in both cases of tissue from GM-CSF K/O mice compared to controls which we quantified in Table 1. Lavaged lung shows a huge increase in the GM-CSF K/O signal compared to controls (Table 1). The increase in lipid content is equally profound for liver from GM-CSF K/O mice compared to controls (Table 1). While the overall increase in lipid droplets is clear, a change in size distribution is also observed. In both lung and liver tissue there is an increase in the relative number of medium and large lipid droplets compared to small lipid droplets.

SHG Microscopy

SHG imaging is well established for imaging collagen fibrillar structures in cells and tissues (30). In this work SHG imaging was carried out simultaneously with CARS microscopy. Thus signals from the same areas were routinely acquired (Table E1). Unexpectedly, the collagen amount and distribution increased significantly in both GM-CSF KO lung and liver consistent with fibrotic damage accompanying lipid accumulation in both tissues. Liver fibrosis was confirmed histologically in GM-CSF KO animals by use of Sirius Red staining (Figure E4) showing both hepatic terminal venule fibrosis as well as a more diffuse collagen fibre deposition evident throughout the tissue. Lavaged lung slices could not be efficiently retained on slides during staining and so were not amenable to histology.

TEM

TEM of lung sections (Figure 7A, 7B) confirmed observations from ORO staining and CARS imaging but also provided information on the spatial distribution of lipid at individual cell level. Lavaged lung tissue did not respond well to TEM fixation and so unlavaged lungs were used. In

AJRCMB Articles in Press. Published on 10-May-2017 as 10.1165/rcmb.2016-0242OC

normal, unlavaged lung (Figure 7A) there was no evidence of lipid droplet accumulation alongside LBs in AT2 cells or in AT1 epithelia or lipofibroblasts, while in the unlavaged lungs from GM-CSF KO animals lipid droplets can clearly be seen to be confined to lipofibroblast cells with no obvious AT2/AT1 accumulation (Figure 7B and Figure E5). Taken together these data identify lipofibroblast cells as the site of a major accumulation of potentially lipotoxic neutral lipid in the GM-CSF animals.

For control liver (Figure 7C), the majority of lipid material present is estimated in a size range consistent with VLDL particles previously recorded for murine VLDL (31). In the case of GM-CSF KO animals, livers show at least three type of lipid particle. In addition to likely nascent VLDL sized lipids there are larger lipid droplets with many clearly bounded by a lipid bilayer (Figure 7D & 7E). These would be consistent with macrovesicular lipid droplets. At higher magnification (Figure 7E) it is clear that there are significant “bunch of grape-like” clusters of very small, microvesicular lipid droplets throughout the cytoplasm of hepatocytes. The accumulation of hepatic lipid in this PAP-linked steatosis is largely confined to hepatocytes with no apparent Kupffer cell involvement.

Discussion

Homeostatic regulation in metabolic systems ensures that they maintain equilibrium within a normal range of values when challenged by external stressors. For lipid metabolism it is the combination of lipid uptake, synthesis, degradation/turnover and export that is balanced in order to preserve cell and tissue integrity without lipid excess or deficit. Any large and sustained change in one or more of those factors has the potential to shift the equilibrium position beyond an organism’s ability to compensate effectively. This is evident for the deranged surfactant metabolism characteristic of PAP (10). In PAP, the lung lipid metabolism steady state position lies significantly outside of the normal range. So, as a result of defective AM function and an associated accumulation of excess lipoproteinaceous material, it is unsustainable without therapeutic intervention(s) that target removal of alveolar surfactant congestion. Unsurprisingly, therefore, many PAP studies address the respiratory sequelae stemming from compromised or blocked alveolar gas exchange capacity. Detailed lipidomic evaluation of pulmonary tissue PC synthesis, secretion and turnover in PAP and any distal tissue sequelae, have not been well documented.

Our lipidomic analyses of lungs and livers and use of complementary modes of histopathology confirmed much of what was already known. In addition we extended and identified new phenotypic characteristics previously unavailable. GM-CSF ablation, in addition to producing substantial accumulations in BALF surfactant and AM accretion of lipotoxic material, is characterised by tissue lipotoxicity in both whole lung and liver tissue. In particular, the steatoses in lipofibroblast cells and whole liver of GM-CSF KO animals are novel observations in this model, as is the pattern of associated liver fibrosis shown by SHG. Moreover, the increased flux through lung PC biosynthesis was unexpected and in the light of previous observations (11) suggests that increased basolateral secretion of PUFA-enriched PC from the lungs likely accompanies GM-CSF ablation.

The PAP-associated, parallel accumulations in whole lung PC and liver PC are striking without immediately obvious rationale for linkage. The simplest explanation is coincidence. Lung and liver both synthesise mixed composition PC species but retain predominantly saturated and unsaturated molecular species respectively, reflecting the distinct requirements of each tissue to maintain appropriate lipid synthesis and secretion capacity. Lung requires saturated PC for pulmonary surfactant production while liver needs unsaturated PC species for very low density lipoprotein (VLDL) construction and secretion. The obvious explanation, however, cannot account for the GM-CSF KO-associated increase in liver PC as well as the enrichment on PUFA-containing PE species seen (supplementary Fig 2) and which is the substrate for PE N-methylation pathway of PC biosynthesis (32). An alternative teleology, involving highly regulated interaction between the two organs and comprising complementary lipid exchange in order to ensure optimal resource and energy utilisation, has not attracted prior exploration. However, the emerging pattern of data from lipidomic studies begins to point to a likely coordination of mechanisms which, at least indirectly, intimately link the PC metabolism of both organs. Moreover, it suggests that significant perturbation of PC homeostasis at the level of one organ, such as that manifest in the PAP lung, may in turn have dramatic consequences for whole body PC/lipid metabolism.

Lung synthesises, enriches and transiently stores, prior to secretion, DSPC as LB surfactant (20). The absolute amounts of lung PC synthesised *in vivo* exceed whole lung requirements by an order of magnitude (19) with the excess, unsaturated PC not destined for alveolar secretion, being returned via a basolateral route (25, 33, 34) to the circulation. Indeed, lung itself may be second only

AJRCMB Articles in Press. Published on 10-May-2017 as 10.1165/rcmb.2016-0242OC

to the liver in the secretion of PUFA-rich lipoprotein into the circulation, albeit as HDL destined for liver recycling rather than VLDL. Liver amasses, through a mix of synthesis *de novo* via the N-methylation pathway (24) and salvage from lipoprotein remnants including HDL (32), PUFA-rich PC for VLDL construction prior to distribution via the circulation (32). More saturated hepatic PC species predominantly synthesised through the CDPcholine pathway (24) are segregated and preferentially secreted with the bile (40). Accordingly, unlike the majority of organs, lung and liver are each responsible for the secretion or export of significant amounts of both saturated and unsaturated PC.

Given these observations and despite established demonstrations of anterograde (via VLDL) and retrograde (via HDL) lipid transfer capacity that link both organs, it is surprising that little attention focuses on any coordination potential between them. Our data adds weight to the possibility that these spatially segregated but apparently complementary phenomena operate in concert.

Newly synthesised lung PC does not display the same extent of saturation enrichment characteristic of the mature, secreted surfactant PC pool (20). Instead, progressive enrichment of saturated PC species operates to achieve the final surfactant PC composition in the alveolar space, a process referred to as remodelling. The conventional understanding of remodelling derives largely from work with cell-free homogenates (35-37) rather than quantitative studies *in vivo*. It sees the main route to saturation enrichment as a molecule-level, post synthesis acyl exchange process removing unsaturated fatty acids followed by an acylCoA-dependent saturated fatty acid replacement (35, 36). However, our data (19) mean that, in the mouse *in vivo*, a sufficient synthesis of surfactant DSPC *de novo* is continuously maintained *in vivo* and is able to keep pace with physiological demand. There is no need *a priori* to resort to the conventional interpretation of significant acyl chain remodelling of newly synthesised material (35, 36) provided that the newly synthesised unsaturated PC excess is quickly exported from the lung. This startling, but experimentally verified observation presents a puzzle; how is that excess unsaturated PC recycled away from the lung?

Even under normal metabolic parameters, steady state enrichment of surfactant DSPC in the lung requires that the significant excess of newly synthesised PUFA enriched PC is removed from the lung environs. PC remodelling in this excess synthesis scenario therefore becomes a high capacity, selective PUFA-enriched PC species removal process rather than a high volume breakdown and reconstruction mechanism. In addition to being more energetically efficient, this would designate the

established acyl-remodelling mechanism as means to correct and tidy mis-directed “mistakes” and effectively tailor LB compositions for purpose.

PUFA-rich PC export from AT2 cells involves basolateral transport to nascent HDL particles subsequently returned to the liver for reuptake and recycling. Retrograde transport of PC facilitates HDL construction and reverse cholesterol transport from peripheral tissues (38). Export of excess polyunsaturated PC likely accompanies cholesterol secretion via basolateral transport. Two ABC transporter proteins, ABCA1 and ABCG1, with recognised roles in cholesterol and phospholipid homeostasis (39), are expressed in both AM and lung epithelia. Murine ABCA1 knockout (40) or ABCG1 knockout (41) each results in a phenotype resembling PAP, with alveolar proteinosis and lung accumulation of surfactant and neutral lipid. Moreover, both functional ABCA1 and ABCG1 appear to be required in AM and epithelia for effective alveolar lipid management, since the increases in AM ABCA1 following ABCG1 ablation do not rescue the phenotype (42). AMs from human patients with PAP also have decreased levels of ABCG1 expression and increased ABCA1 supporting this idea (42). Furthermore, these studies have shown that cholesterol efflux to pre-formed HDL specifically requires ABCG1, whereas efflux to apoA1 requires ABCA1 (43).

The HDL returned from lung to liver likely arises both from lipid transfer to circulating nascent lipoprotein and via *in situ* construction *de novo* from lung tissue synthesised Apo-A1 (44). Capacity for the latter exists in humans and mice and operates with increases in circumstances where surfactant is known to accumulate (45) including perinatal surges in surfactant synthesis and storage where synchronous increases in lung parenchymal Apo-A1 mRNA production occur (44, 45).

The elevated unsaturated PC content in the liver, following GM-CSF ablation, suggests either a reduced rate of lipoprotein secretion resulting in a larger, un-secreted pool or an increased rate of re-uptake of HDL enlarging the steady-state pool. Quantitative assessments of the hepatic uptake of HDL particles have established that 50% of the HDL PC PUFA is directed to transient TAG storage while the other half is directly reclaimed for VLDL construction and secretion (32). Any shift in the equilibrium position that would accompany even small but sustained increases in HDL uptake outside of the normal range could mandate larger transient PC and TAG pools. Once of sufficient magnitude, steatosis may result. Our data strongly point to a mixed steatotic pattern in the liver of GM-CSF KO animals whereby both microvesicular and macrovesicular characteristics are apparent.

AJRCMB Articles in Press. Published on 10-May-2017 as 10.1165/rcmb.2016-0242OC

Fibrotic damage, evident from the collagen fibrils seen in both lung and liver, reflects that seen elsewhere in lipotoxicity (46) pointing to sustained inflammatory responses to lipid accumulation that leads to injurious consequence. Interestingly, this hepatic damage in PAP may have a reciprocal relationship, seen in the lung and AM lipotoxicity reported in an alcoholic liver cirrhosis model (47). The PAP literature suggests that hepatic pathology is not a recognised phenomenon, most likely due to minimal prior exploration of the possibility. However, reported human PAP pathology, at least in one in a specific genetic cohort, includes a hepatomegaly component which may stem from lipid accumulation and relate to our observations (48). Moreover, a study of bleomycin-induced fibrosis shows that liver steatosis can arise alongside the lipid metabolism changes that follow lung damage and tissue repair (49). These add further weight to a coordinated hepato-pulmonary axis of lipid metabolism Deranged hepato-pulmonary coordination of lipid metabolism may be a common phenomenon that merits closer examination in both primary lung and liver diseases.

Acknowledgements

Thanks to Mr Jon Ward, Histochemistry Research Unit, University of Southampton for OCT embedding and cutting of tissues and ORO and Sirius red staining and to Dr Anton Page, Biomedical Imaging Unit, University of Southampton for sample processing for, and assistance with, TEM. The mass spectrometry elements of this work were supported by an equipment grant from The Wellcome Trust reference 057405

References

1. Jackowski S. Cell cycle regulation of membrane phospholipid metabolism. *J Biol Chem* 1996;271:20219-22
2. Unger RH, Clark GO, Scherer PE, Orci L. Lipid homeostasis, lipotoxicity and the metabolic syndrome. *Biochim Biophys Acta*. 2010;1801:209-14.
3. Szendroedi J, Roden M. Ectopic lipids and organ function. *Curr Opin Lipidol.* 2009;20:50-6
4. Haffar T, Bérubé-Simard F, Bousette N. Impaired fatty acid oxidation as a cause for lipotoxicity in cardiomyocytes. *Biochem Biophys Res Commun.* 2015;468:73-8.

5. Guebre-Egziabher F, Alix PM, Koppe L, Pelletier CC, Kalbacher E, Fouque D, Soulage CO. Ectopic lipid accumulation: A potential cause for metabolic disturbances and a contributor to the alteration of kidney function. *Biochimie.* 2013;95:1971-9.
6. Gaemers IC, Stallen JM, Kunne C, Wallner C, van Werven J, Nederveen A, Lamers WH. Lipotoxicity and steatohepatitis in an overfed mouse model for non-alcoholic fatty liver disease. *Biochim Biophys Acta.* 2011;1812:447-58.
7. Turpin SM, Ryall JG, Southgate R, Darby I, Hevener AL, Febbraio MA, Kemp BE, Lynch GS, Watt MJ. Examination of 'lipotoxicity' in skeletal muscle of high-fat fed and ob/ob mice. *J Physiol.* 2009;587:1593-605.
8. Kochan K, Maslak E, Krafft C, Kostogrys R, Chlopicki S, Baranska M. Raman spectroscopy analysis of lipid droplets content, distribution and saturation level in Non-Alcoholic Fatty Liver Disease in mice. *J Biophotonics.* 2015;8:597-609.
9. Mota M, Banini BA, Cazanave SC, Sanyal AJ. Molecular mechanisms of lipotoxicity and glucotoxicity in nonalcoholic fatty liver disease. *Metabolism.* 2016;65:1049-61.
10. Carey B, Trapnell BC. The molecular basis of pulmonary alveolar proteinosis. *Clin Immunol.* 2010;135:223-35.
11. Trapnell BC, Carey BC, Uchida K, Suzuki T. Pulmonary alveolar proteinosis, a primary immunodeficiency of impaired GM-CSF stimulation of macrophages. *Curr Opin Immunol.* 2009;21:514-21.
12. Dranoff G, Crawford AD, Sadelain M, Ream B, Rashid A, Bronson RT, Dickersin GR, Bachurski CJ, Mark EL, Whitsett JA, Mulligan RC. Involvement of granulocyte-macrophage colony-stimulating factor in pulmonary homeostasis. *Science.* 1994;264:713-6.
13. Ikegami M, Ueda T, Hull W, Whitsett JA, Mulligan RC, Dranoff G, Jobe AH. Surfactant metabolism in transgenic mice after granulocyte macrophage-colony stimulating factor ablation. *Am J Physiol.* 1996;270:L650-8.
14. Baker AD, Malur A, Barna BP, Ghosh S, Kavuru MS, Malur AG, Thomassen MJ. Targeted PPARγ deficiency in alveolar macrophages disrupts surfactant catabolism. *J Lipid Res.* 2010;51:1325–1331

AJRCMB Articles in Press. Published on 10-May-2017 as 10.1165/rcmb.2016-0242OC

15. Malur A, Baker AD, McCoy AJ, Wells G, Barna BP, Kavuru MS, Malur AG, Thomassen MJ. Restoration of PPARγ reverses lipid accumulation in alveolar macrophages of GM-CSF knockout mice. *Am J Physiol Lung Cell Mol Physiol.* 2011;300:L73-80. .
16. Foster DJ, Ravikumar P, Bellotto DJ, Unger RH, Hsia CC. Fatty diabetic lung: altered alveolar structure and surfactant protein expression. *Am J Physiol Lung Cell Mol Physiol.* 2010;298:L392-403
17. Plantier L, Besnard V, Xu Y, Ikegami M, Wert SE, Hunt AN, Postle AD, Whitsett JA. Activation of sterol-response element-binding proteins (SREBP) in alveolar type II cells enhances lipogenesis causing pulmonary lipotoxicity. *J Biol Chem.* 2012;287:10099-114.
18. Besnard V, Wert SE, Stahlman MT, Postle AD, Xu Y, Ikegami M, Whitsett JA. Deletion of Scap in alveolar type II cells influences lung lipid homeostasis and identifies a compensatory role for pulmonary lipofibroblasts. *J Biol Chem.* 2009;284:4018-30.
19. Postle AD, Henderson NG, Koster G, Clark HW, Hunt AN. Analysis of lung surfactant phosphatidylcholine metabolism in transgenic mice using stable isotopes. *Chem Phys Lipids.* 2011;164:549-55.
20. Goss V, Hunt AN, Postle AD. Regulation of lung surfactant phospholipid synthesis and metabolism. *Biochim Biophys Acta.* 2013;1831:448-58.
21. McKenzie Z, Kendall M, Mackay RM, Whitwell H, Elgy C, Ding P, Mahajan S, Morgan C, Griffiths M, Clark H, Madsen J. Surfactant protein A (SP-A) inhibits agglomeration and macrophage uptake of toxic amine modified nanoparticles. *Nanotoxicology*. 2015;9:952-62.
22. Schneider CA, Rasband WS, Eliceiri KW. NIH Image to ImageJ: 25 years of image analysis. *Nature methods* 2012;9:671-675
23. Hunt AN, Clark GT, Attard GS, Postle AD. Highly saturated endonuclear phosphatidylcholine is synthesized in situ and colocated with CDP-choline pathway enzymes. *J Biol Chem.* 2001;276:8492-9.
24. Pynn CJ, Henderson NG, Clark H, Koster G, Bernhard W, Postle AD. Specificity and rate of human and mouse liver and plasma phosphatidylcholine synthesis analyzed in vivo. *J Lipid Res.* 2011;52:399-407
25. Zhou J, You Y, Ryan AJ, Mallampalli RK. Upregulation of surfactant synthesis triggers ABCA1-mediated basolateral phospholipid efflux. *J Lipid Res.* 2004;45:1758-67.

26. Cole LK, Vance JE, Vance DE. Phosphatidylcholine biosynthesis and lipoprotein metabolism. *Biochim Biophys Acta.* 2012;1821:754-61

27. Patel II, Steuwe C, Reichelt S, Mahajan S. Coherent anti-Stokes Raman scattering for label-free biomedical imaging. J Optics 2013;15: 094006 DOI: 10.1088/2040-8978/15/9/094006

28. Gao L, Wang Z, Li F, Hammoudi AA, Thrall MJ, Cagle PT, Wong ST. Differential diagnosis of lung carcinoma with coherent anti-Stokes Raman scattering imaging. *Arch Pathol Lab Med.* 2012;136:1502-10.

29. Le TT, Ziemba A, Urasaki Y, Brotman S, Pizzorno G. Label-free evaluation of hepatic microvesicular steatosis with multimodal coherent anti-Stokes Raman scattering microscopy. *PLoS One.* 2012;7:e51092. doi: 10.1371/journal.pone.0051092.

30. Zoumi A, Yeh A, Tromberg BJ. Imaging cells and extracellular matrix in vivo by using second-harmonic generation and two-photon excited fluorescence. *Proc Natl Acad Sci U S A.* 2002;99:11014-9.

31. Werner A, Havinga R, Bos T, Bloks VW, Kuipers F, Verkade HJ. Essential fatty acid deficiency in mice is associated with hepatic steatosis and secretion of large VLDL particles. *Am J Physiol Gastrointest Liver Physiol.* 2005;288:G1150-8.

32. Vance DE. Role of phosphatidylcholine biosynthesis in the regulation of lipoprotein homeostasis. *Curr Opin Lipidol.* 2008;19:229-34

33. Bates SR, Tao JQ, Collins HL, Francone OL, Rothblat GH. Pulmonary abnormalities due to ABCA1 deficiency in mice. *Am J Physiol Lung Cell Mol Physiol.* 2005;289:L980-9..

34. Bates SR, Tao JQ, Yu KJ, Borok Z, Crandall ED, Collins HL, Rothblat GH. Expression and biological activity of ABCA1 in alveolar epithelial cells. *Am J Respir Cell Mol Biol.* 2008;38:283-92

35. Tsao FH, Zachman RD. Phosphatidylcholine-lysophosphatidylcholine cycle pathway enzymes in rabbit lung. I. Subcellular localization and properties. *Pediatr Res.* 1977;11:849-57.

36. Caesar PA, McElroy MC, Kelly FJ, Normand IC, Postle AD. Mechanisms of phosphatidylcholine acyl remodeling by human fetal lung. *Am J Respir Cell Mol Biol.* 1991;5:363-70.

AJRCMB Articles in Press. Published on 10-May-2017 as 10.1165/rcmb.2016-0242OC

37. Chen X, Hyatt BA, Mucenski ML, Mason RJ, Shannon JM. Identification and characterization of a lysophosphatidylcholine acyltransferase in alveolar type II cells. *Proc Natl Acad Sci U S A.* 2006;103:11724-9

38. Zhao GJ, Yin K, Fu YC, Tang CK. The interaction of ApoA-I and ABCA1 triggers signal transduction pathways to mediate efflux of cellular lipids. *Mol Med.* 2012;18:149-58

39. Phillips MC. Molecular mechanisms of cellular cholesterol efflux. *J Biol Chem.* 2014;289:24020-9.

40. Bates SR, Tao JQ, Collins HL, Francone OL, Rothblat GH. Pulmonary abnormalities due to ABCA1 deficiency in mice. *Am J Physiol Lung Cell Mol Physiol.* 2005;289:L980-9.

41. Baldán A, Gomes AV, Ping P, Edwards PA. Loss of ABCG1 results in chronic pulmonary inflammation. *J Immunol.* 2008;180:3560-8.

42. Thomassen MJ, Barna BP, Malur A, Bonfield TL, Farver CF, Malur A, Dalrymple H, Kavuru MS and Febbraio M. ABCG1 is deficient in alveolar macrophages of GM-CSF knock-out mice and patients with pulmonary alveolar proteinsosis. *J Lipid Res* 2007;48:2762-2768.

43. Kennedy MA, Barrera GC, Nakamura K, Baldan A, Tarr P, Fishbein MC, Frank J, Francone OL and Edwards PA. ABCG1 has a critical role in mediating cholesterol efflux to HDL and preventing cellular lipid accumulation. *Cell Metabolism* 2005;1:121-131

44. Côté M, Provost PR, Tremblay Y. Apolipoprotein A-I, A-II, and H mRNA and protein accumulation sites in the developing lung in late gestation. *BMC Res Notes.* 2011;4:235.

45. Provost PR, Tremblay Y. Elevated expression of four apolipoprotein genes during the 32-35 week gestation window in the human developing lung. *Early Hum Dev.* 2010;86:529-34

46. Brackmann C, Gabrielsson B, Svedberg F, Holmaang A, Sandberg AS, Enejder A. Nonlinear microscopy of lipid storage and fibrosis in muscle and liver tissues of mice fed high-fat diets *J Biomed Opt.* 2010;15:066008. doi: 10.1117/1.3505024.

47. Romero F, Shah D, Duong M, Stafstrom W, Hoek JB, Kallen CB, Lang CH, Summer R. Chronic alcohol ingestion in rats alters lung metabolism, promotes lipid accumulation, and impairs alveolar macrophage functions. *Am J Respir Cell Mol Biol.* 2014;51:840-9.

48. Enaud L, Hadchouel A, Coulomb A, Berteloot L, Lacaille F, Boccon-Gibod L, Boulay V, Darcel F, Griese M, Linard M, Louha M, Renouil M, Rivière JP, Toupance B, Verkarre V, Delacourt C,

de Blic J. Pulmonary alveolar proteinosis in children on La Réunion Island: a new inherited disorder? *Orphanet J Rare Dis.* 2014 Jun 14;9:85. doi: 10.1186/1750-1172-9-85.

49. Hu C, Wang Y, Fan Y, Li H, Wang C, Zhang J, Zhang S, Han X, Wen C. Lipidomics revealed idiopathic pulmonary fibrosis-induced hepatic lipid disorders corrected with treatment of baicalin in a murine model. *AAPS J.* 2015;17:711-22

AJRCMB Articles in Press. Published on 10-May-2017 as 10.1165/rcmb.2016-0242OC

		CARS image intensity ± S.D. (per image FOV)	Size (% of total number of lipid droplets)		
			<1 μm^2 (small)	1-5 μm^2 (medium)	>5 μm^2 (large)
Lavaged Lung	Control	107.7 ± 34.4	72.3	25.2	2.5
	GMCSF -KO	300.7 ± 34.2	70.7	25.2	4.1
Liver	Control	193.1 ± 49.9	80.3	18.9	0.8
	GMCSF -KO	413.5 ± 235.3	68.7	26.6	4.7

Table 1 CARS Quantification

From 3 samples each of control and GM-CSF KO lung and liver tissues, 10 fields of view (FOV) were selected (ie 30 for each group) and subjected to CARS imaging. Upon subsequent image analyses the distribution of lipid droplets was characterised using arbitrary size ranges broadly defined as small, medium and large. CARS image intensity reflects lipid concentration permitting semi-quantitative assessment of total lipid change. Increases in total lipid and droplet sizes are readily apparent in both lungs and livers of GM-CSF KO animals.

Figure Legends

Figure 1. PC accumulations in lung compartments. The mean PC content of control samples were defined as 100% ± SEM while increased content of equivalent samples from GM-CSF ablated animals expressed as a percentage of relevant control mean ± SEM. (Lavaged lung n = 12 & 24, BALF n = 9 &19, Recovered cells n = 11 & 14)

Figure 2. PC molecular species compositions in lung compartments. Panel A shows the proportional representation of all PC species >0.5% total PC in lavaged lung tissue from control and GM-CSF KO animals (mean ± SEM, n = 12 & 24). Panel B shows the proportional representation of all PC species >0.5% total PC in BALF from control and GM-CSF KO animals (mean ± SEM, n = 9 &19). Panel C shows the proportional representation of all PC species >0.5% total PC in cells recovered from control and GM-CSF BALF (mean ± SEM, n = 11 & 14). Reported molecular species represented the experimentally ascertained dominant molecular species from the potential isobaric options.

Figure 3. PC molecular species compositions and contents of whole liver. Panel A shows **t**he proportional representation of all PC species >0.5% total PC in whole liver from control and GM-CSF KO animals (mean ± SEM, n = 8 & 20) consistent with relative enrichment of polyunsaturated PC. However, panel B shows the contents of the same molecular species per gram wet weight liver. With the exception of PC16:0/18:2 all PC species were elevated significantly in GM-CSF livers as shown were polyunsaturated.

Figure 4. Oil Red O staining of lavaged lung sections and liver sections. Lavaged lung and liver samples were stained with ORO, counterstained with Mayer's Haematoxylin and observed using a x100 oil immersion lens. Panel A shows a representative control lavaged lung section with sporadic ORO stained inclusions. Panel B shows a representative GM-CSF lavaged lung with many more ORO stained inclusions apparently in AT1 respiratory epithelia. Panel C shows a representative control liver section with ORO stained droplets distributed largely in the sinusoids. Panel D shows a representative GM-CSF liver section with widespread ORO stained lipid droplet inclusions of varying size within hepatocytes as well as sinusoids, a pattern consistent with steatosis.

AJRCMB Articles in Press. Published on 10-May-2017 as 10.1165/rcmb.2016-0242OC

Figure 5. CARS and SHG of lung sections. Lavaged lungs from control and GM-CSF KO animals were subject to CARS and SHG microscopy as described. Panels A & B show CARS images which confirm significant increases in lipid droplets present in GM-CSF lungs. Panels E & F show the SHG images of the same areas which show a pattern of increased collagen fibres in the GM-CSF KO lungs. Panels C & D show the respective image merges and defining the spatial relationships between lipid accretion and fibrotic changes.

Figure 6. CARS and SHG of liver sections. Livers from control and GM-CSF KO animals were subject to CARS and SHG microscopy as described. Panels A & B show CARS images which confirm significant increases in number and size of lipid droplets present in GM-CSF livers. Panels E & F show the SHG images of the same areas which show a pattern of significantly increased collagen fibre depositions in the GM-CSF KO livers. Panels C & D show the respective image merges and defining the spatial relationships between lipid accretion and hepatic fibrotic changes.

Figure 7. TEM of lung and liver tissues. Unlavaged lungs and livers from control and GM-CSF KO animals were subjected to TEM as described. For control lungs 12 distinct image fields were collected and analysed from 3 grids. For GM-CSF KO lungs 17 distinct image fields were collected and analysed from 4 grids. For control livers 9 distinct image fields were collected and analysed from 3 grids with 12 distinct image fields collected and analysed from 4 grids. Scale bars for lung tissue are 2000nm and for liver tissue 5000nm. Control lung, panel A is representative and shows a few sporadic lipid droplets indicated by arrows but no consistent pattern. By contrast, panel B is representative and shows accumulations of lipid droplets largely confined to lipofibroblast cells with no indication of involvement of the adjacent AT2 or AT1 cells. A larger version of panel B is presented in supplementary material (Figure E5) showing more detailed labelling of cells and lipid contents. Control liver, panel C, is representative and shows a number of lipid droplets (red arrows) present some representing nascent lipoproteins and others more likely lipid stores. The GM-CSF KO liver, panel D, is representative and by contrast shows a much wider range of lipid droplets (red arrows) which in addition to lipoproteins reveal, when zoomed in upon in panel E, clusters of very small droplets (outlined in red) alongside larger droplets bounded by lipid bilayers.

AJRCMB Articles in Press. Published on 10-May-2017 as 10.1165/rcmb.2016-0242OC

Figure 1

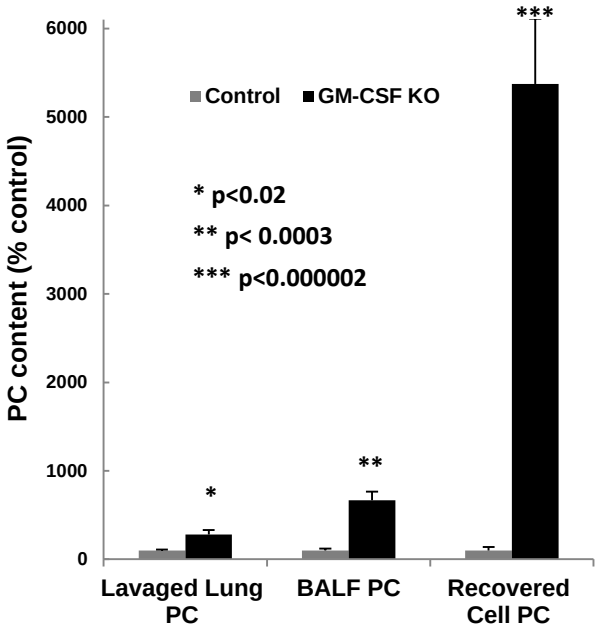

AJRCMB Articles in Press. Published on 10-May-2017 as 10.1165/rcmb.2016-0242OC

Figure 2

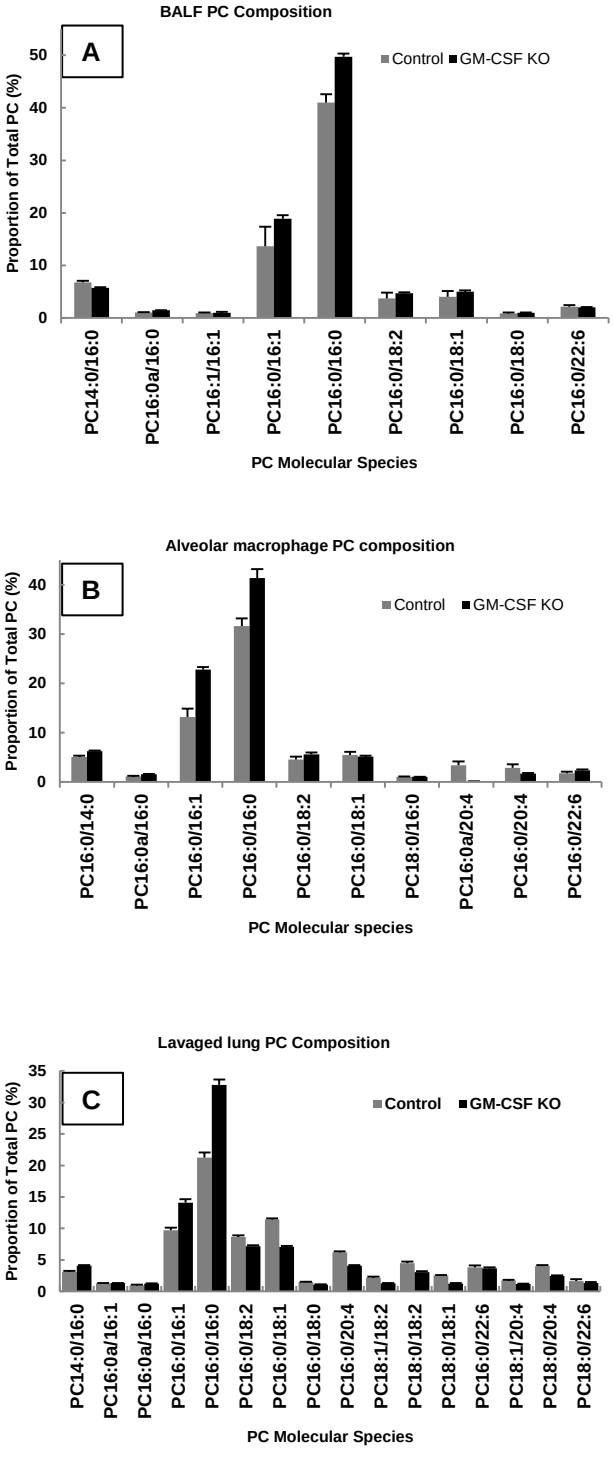

Figure 3

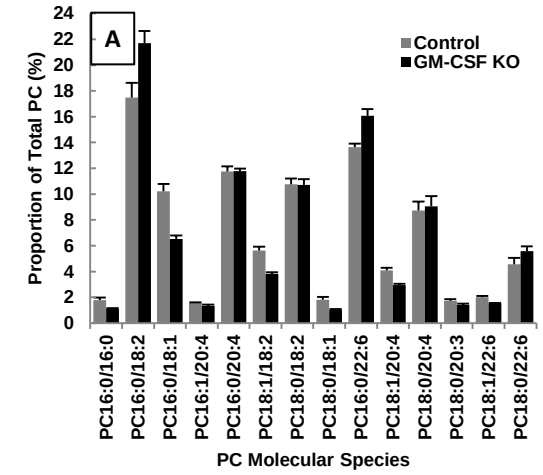

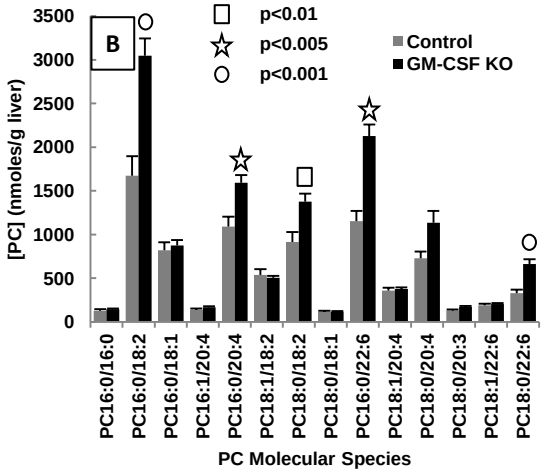

AJRCMB Articles in Press. Published on 10-May-2017 as 10.1165/rcmb.2016-0242OC

Figure 4

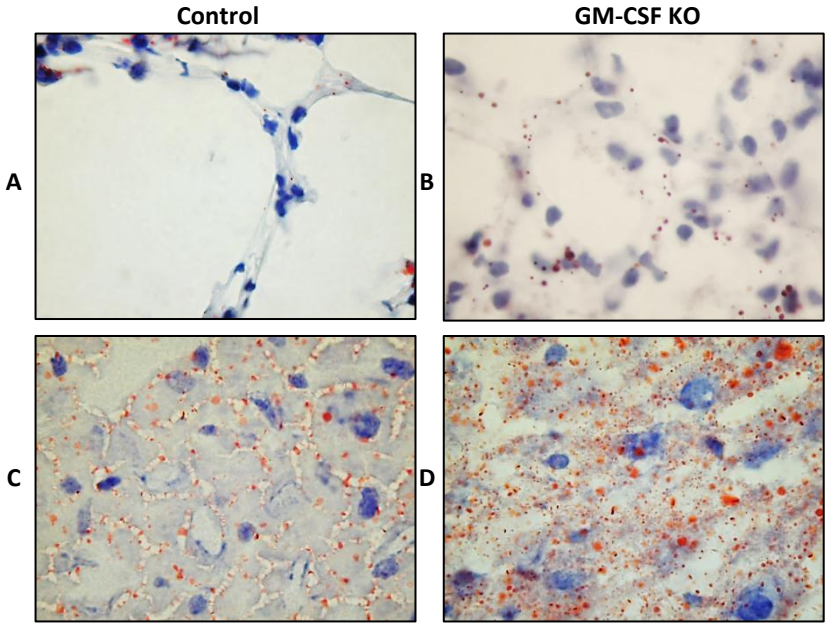

Figure 5

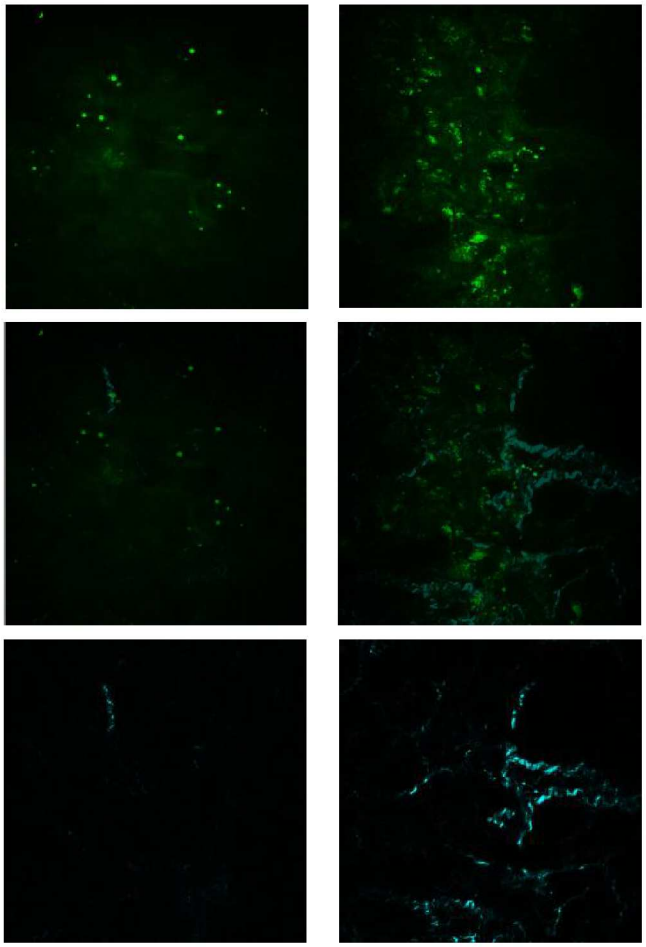

AJRCMB Articles in Press. Published on 10-May-2017 as 10.1165/rcmb.2016-0242OC

Figure 6

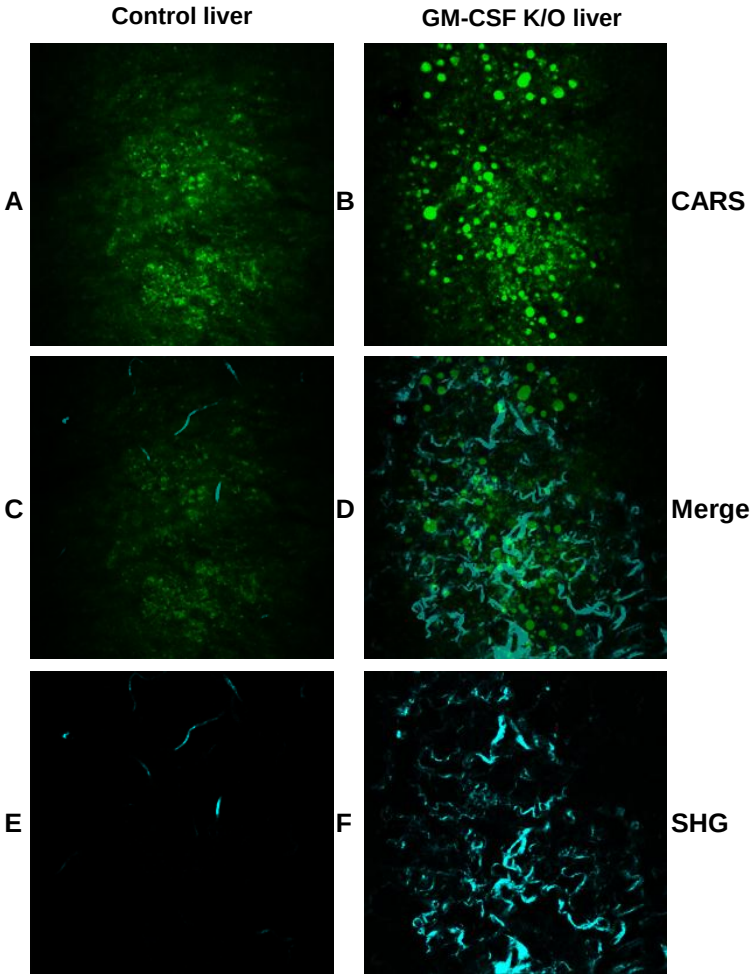

Figure 7

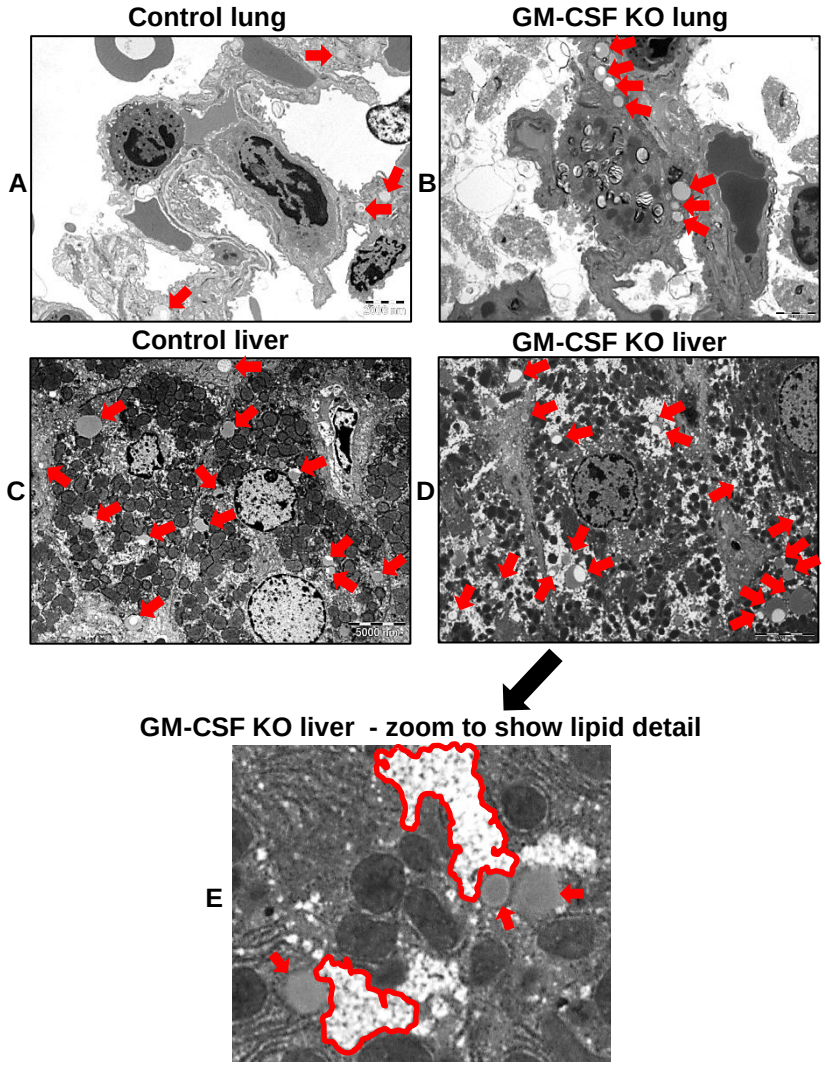

AJRCMB Articles in Press. Published on 10-May-2017 as 10.1165/rcmb.2016-0242OC

Supplementary Figure Legends

Figure E1

Panel A: shows the proportions of diacyl PE species present in lavaged lung tissue from control and GM-CSF KO mice (means ± S.E.M, n = 8 & 20). Unlike tissue PC, there were no significant variations between the groups. This lack of variation was also reflected in the total PE recovered: control [PE] was 2.67 ± 0.19 μmoles/g and GM-CSF KO was 2.23 ± 0.28 μmoles/g (p=0.21).

Panel B: shows the proportions of PI species present in the same tissues. Here, a significant reduction in proportion of PI18:0/20:4 ($p<0.05$) in GM-CSF KO lungs was accompanied by a significant increase in PI16:0/22:6 ($p<0.01$).

PG and PS showed no significant compositional variations (data not shown) and while no internal standards were included for PI, PG, PS, relative intensities compared with other phospholipid classes did not suggest dramatic variations.

Figure E2

Analyses of plasma PC compositions shows two significant proportion increases in the PC16:0/22:6 and PC18:0/22:6 of GM-CSF KO animals (*$p<0.02$ for each, n = 8 & 11). Total plasma [PC] was unaltered between animals

Figure E3

PE molecular species compositions and contents of whole liver. Panel A shows **t**he proportional representation of all PE species >0.5% total PE in whole liver from control and GM-CSF KO animals (mean ± SEM, n = 8 & 20). Panel B shows the contents of the same molecular species per gram wet weight liver. Contents of PE16:0/18:2, PE18:0/18:2, PE16:0/22:6, PE18:020:4 and PE18:0/22:6 were all significantly elevated (<0.02) in GM-CSF livers.

The total liver PE pool is elevated 70.8% from 6.320 ± 0.473 μmoles/g to 10.798 ± 0.407 μmoles/g (means ± SEM, n = 8 & 20, $p<0.01$

Figure E4

Sirius red staining of control and GM-CSF KO mouse livers (x40 magnification)

Staining of collagen in control and GM-CSF KO animal livers shows (i) minimal evidence of fibrotic damage in controls (A-C), whereas (ii) GM-CSF animals show both hepatic terminal venule fibrosis (D & F) as well as a more diffuse collagen fibre deposition (E) evident throughout the tissue (D-F)

Figure E5

Ultrastructural TEM image of Lipid Droplet (LD) distribution in GM-CSF KO lungs

AT1 – Alveolar type I cell, AT2 – Alveolar type II cell, AM – Alveolar macrophage, LF – Lipofibroblast, CAP – Capillary, LB – Lamellar body, LD – Lipid droplet

AJRCMB Articles in Press. Published on 10-May-2017 as 10.1165/rcmb.2016-0242OC

		SHG image intensity ± S.D. (per image FOV)
Lavaged Lung	Control	64.74 ± 0.39
	GMCSF -KO	*71.04 ± 5.38
Liver	Control	68.27 ± 0.99
	GMCSF -KO	**76.04 ± 9.77

Table E1 SHG Quantification

From 3 samples each of control and GM-CSF KO lung and liver tissues, 10 fields of view (FOV) were selected (ie 30 for each group) and subjected to SHG imaging for collagen fibres. SHG image intensity reflects the presence of collagen fibres permitting semi-quantitative assessment of fibrotic change. Increases in total fibrosis are apparent in both lungs and livers of GM-CSF KO animals. Non-parametric data *$p<0.0001$, **$p<0.001$, Mann-Whitney

Figure E1

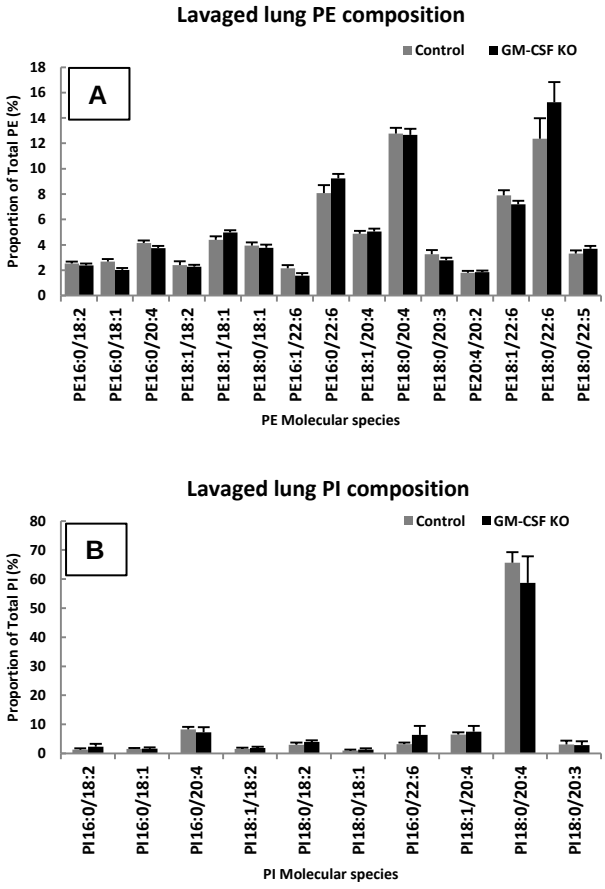

AJRCMB Articles in Press. Published on 10-May-2017 as 10.1165/rcmb.2016-0242OC

Figure E2

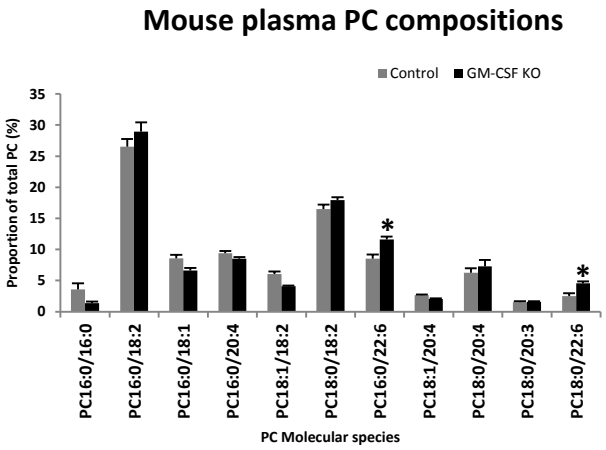

Figure E3

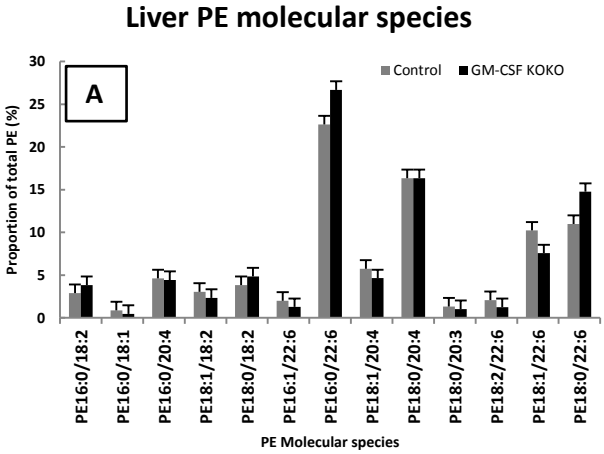

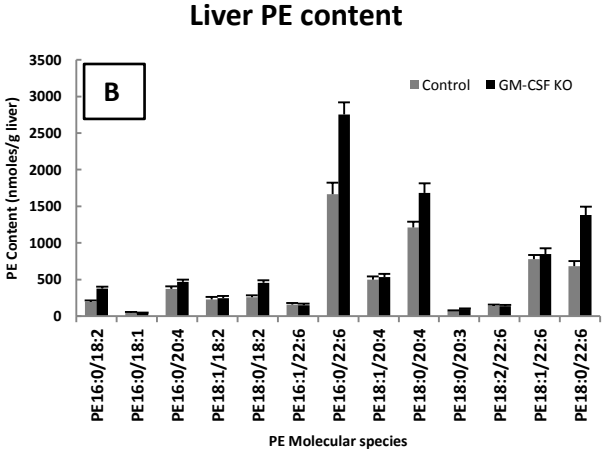

AJRCMB Articles in Press. Published on 10-May-2017 as 10.1165/rcmb.2016-0242OC

Figure E4

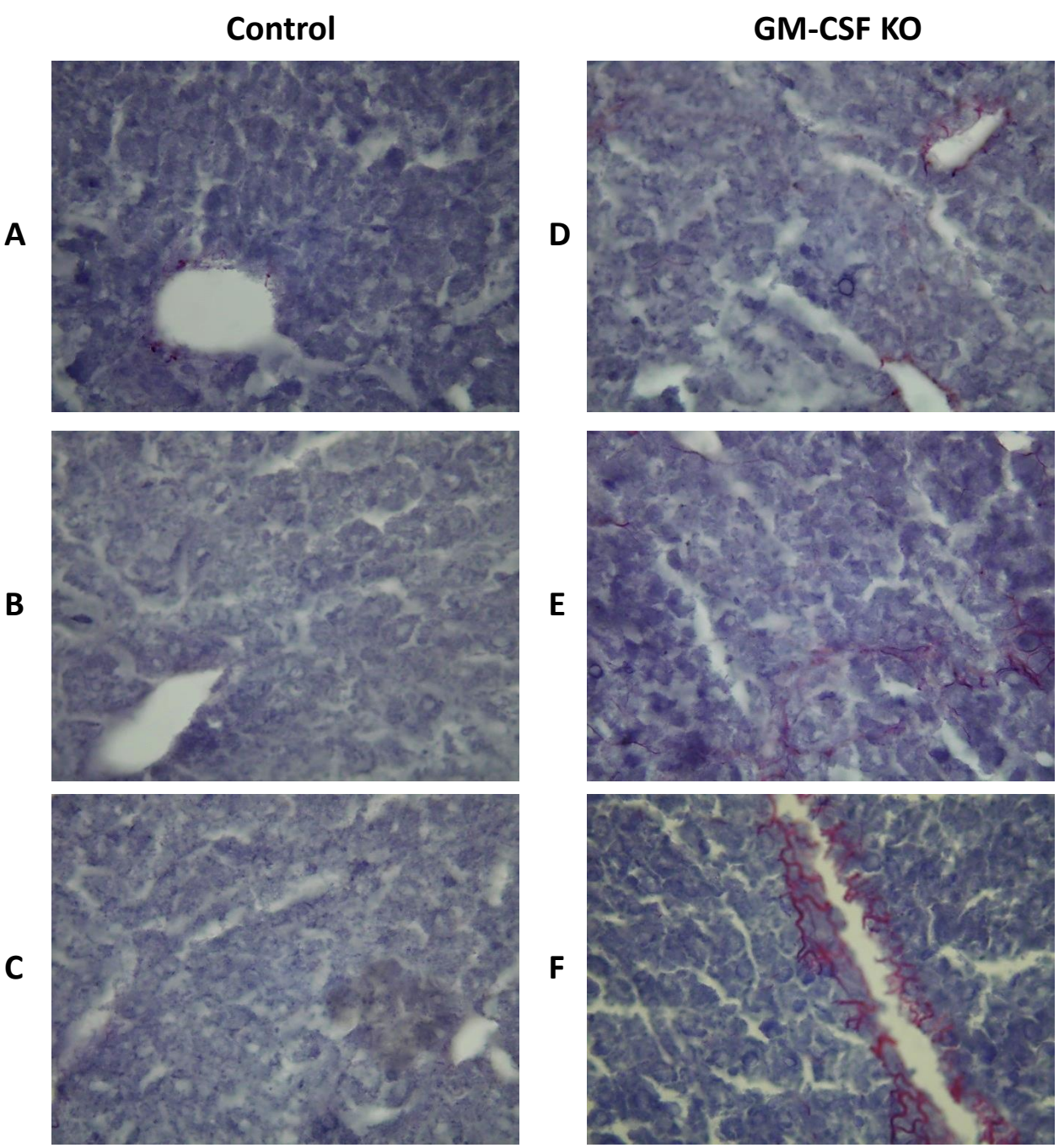

Figure E5